



# Cation deficiency enabled fast oxygen reduction reaction for a novel SOFC cathode with promoted CO<sub>2</sub> tolerance

Xifeng Ding<sup>a,b,\*</sup>, Zhipeng Gao<sup>a,b</sup>, Dong Ding<sup>c</sup>, Xinyu Zhao<sup>a,b</sup>, Huaiyu Hou<sup>a,b</sup>, Shihua Zhang<sup>a,b</sup>, Guoliang Yuan<sup>a,b</sup>

<sup>a</sup> School of Materials Science and Engineering, Nanjing University of Science and Technology, Nanjing, 210094, China

<sup>b</sup> Key Laboratory of Advanced Micro & Nano Materials and Technology in Jiang Province, Nanjing, 210094, China

<sup>c</sup> Redox Power System, College Park, MD, 20742, USA

## ARTICLE INFO

### Keywords:

Solid oxide fuel cells  
Oxygen reduction reaction  
Cation deficiency  
CO<sub>2</sub> tolerance

## ABSTRACT

Cation deficiency in perovskite oxides can alter the crystal structure, oxygen stoichiometry and other physicochemical properties, substantially promote the electro-catalytic activity for oxygen reduction reaction (ORR) at elevated temperatures. In this work, a small strontium deficiency was introduced into SrCo<sub>0.8</sub>Nb<sub>0.1</sub>Ta<sub>0.1</sub>O<sub>3-δ</sub> (S100CNT) to promote the electrochemical activity of ORR. Cation deficient Sr<sub>0.95</sub>Co<sub>0.8</sub>Nb<sub>0.1</sub>Ta<sub>0.1</sub>O<sub>3-δ</sub> (S095CNT) displayed higher oxygen vacancy concentration than that of stoichiometric S100CNT. The decreased average bonding energy (ABE) and the increased critical radius (*r<sub>c</sub>*) of S095CNT could be responsible for the decreased activation energy for oxygen ions transfer. Consequently, the ORR activity of S095CNT cathode was significantly improved. The S095CNT cathode shows an area specific resistance of 0.07 Ω cm<sup>2</sup> at 650 °C, which was only about 63% of S100CNT. Moreover, S095CNT displayed much higher CO<sub>2</sub> tolerance than the state-of-the-art Ba<sub>0.5</sub>Sr<sub>0.5</sub>Co<sub>0.8</sub>Fe<sub>0.2</sub>O<sub>3-δ</sub> (BSCF) cathode for SOFC. Thus, the fast ORR and high stability makes S095CNT promising material for devices involving oxygen electrochemistry such as solid oxide fuel cells, electrolysis cells, or gas separation membranes.

## 1. Introduction

Solid oxide fuel cells (SOFCs) are attractive energy conversion devices due to their highly-efficient electricity generation, flexible fuel sources, and low emissions [1–3]. However, the conventional SOFCs generally operate at high temperatures (800–1000 °C), which leads to high reactivity between cell components and strict requirements on interconnect materials. Consequently, decreasing the operating temperature is an effective means to solve such issues for commercial applications of SOFCs. However, the oxygen reduction reaction (ORR) activity on cathode tends to reduce with the drop of operating temperature. Hence, the exploration of novel cathode materials with high catalytic activity for ORR is of significant importance. Extensive efforts have been undertaken to develop high-performance cathodes in the past decades [4–6].

ABO<sub>3</sub> perovskite-type mixed oxide-ionic and electronic conductors (MIECs) are excellent potential cathodes for low-to-intermediate SOFCs [7–11]. The MIECs can extend the triple phase boundaries (TPBs) to the bulk phase as well as the entire cathode surface [12], leading to a remarkable performance promotion. Among the MIEC oxides, SrCoO<sub>3</sub> –

based cathodes with cubic perovskite structure demonstrated high oxygen ionic and electronic conductivity [13], but low structure stability at high temperature [14]. Many cations, such as Ni, Cu, Zn, Cr, Fe, Al, Ga, In, Ce, Ti, Zr, Sn, V and Nb, were thus doped to stabilize its cubic structure [15]. Among which SrCo<sub>0.9</sub>Nb<sub>0.1</sub>O<sub>3-δ</sub> has the best structure stability and highest oxygen permeation. Moreover, Zhu et al. [16] reported that SrNb<sub>0.1</sub>Co<sub>0.9-x</sub>Fe<sub>x</sub>O<sub>3-δ</sub> exhibited high performance at low temperature ascribing to the formation of oxygen vacancies at high temperature and preserved primitive cubic structure, which substantially improved ORR activity for SOFC cathode.

Introducing cation deficiency into crystal lattice of a compound may alter its original physical and chemical properties, such as phase structure, electrical conductivity and oxygen permeability, as reported in many literatures [17–21]. For example, Shao et al. [22] observed that the A-site cation-deficient compound, Sr<sub>1-x</sub>Nb<sub>0.1</sub>Co<sub>0.9</sub>O<sub>3-δ</sub>, exhibited different space group compared to the cation-stoichiometric SrNb<sub>0.1</sub>Co<sub>0.9</sub>O<sub>3-δ</sub>. Zhao and Kharton et al. [23,24] confirmed increased ionic conductivity of Sr<sub>1-x</sub>Ti<sub>0.60</sub>Fe<sub>0.40</sub>O<sub>3-δ</sub> and (Y<sub>0.08</sub>Sr<sub>0.92</sub>)<sub>1-x</sub>TiO<sub>3-δ</sub> perovskite oxides with the increase of A-site deficiency. Liang et al. [25] observed that A-site cation deficiency effectively increased the oxygen

\* Corresponding author at: School of Materials Science and Engineering, Nanjing University of Science and Technology, Nanjing, 210094, China.

E-mail address: [dingxifeng@njust.edu.cn](mailto:dingxifeng@njust.edu.cn) (X. Ding).

<https://doi.org/10.1016/j.apcatb.2018.10.075>

Received 17 July 2018; Received in revised form 19 October 2018; Accepted 28 October 2018

Available online 06 November 2018

0926-3373/ © 2018 Elsevier B.V. All rights reserved.

non-stoichiometry in  $\text{SrSc}_{0.175}\text{Nb}_{0.025}\text{Co}_{0.8}\text{O}_{3-\delta}$  and substantially facilitated electro-catalytic activity for oxygen reduction. Pang et al. [26] and Donazzi et al. [27] have also demonstrated that polarization resistance could be reduced by introducing Ba-deficiency in the parent  $\text{PrBaCo}_2\text{O}_{5+\delta}$  and  $\text{NdBaCo}_2\text{O}_{5+\delta}$  compounds. The introduction of A-site deficiency tended to create oxygen vacancies and/or to reduce B-site cation valence, and thus facilitated oxygen ionic transport and enhanced the ORR activity [28]. However, thermally-induced lattice oxygen release and the formation of oxygen vacancies would hinder the mobility of electronic conduction carriers and reduce the electronic conductivity of the materials [29]. Thus, an excessive deficiency may be against to promote ORR activity.

In this work, a novel A-site deficient perovskite,  $\text{Sr}_x\text{Co}_{0.8}\text{Nb}_{0.1}\text{Ta}_{0.1}\text{O}_{3-\delta}$  ( $x = 0.90, 0.95, 1.00$ ), were synthesized and investigated as a promising cathode material for low-to-intermediate SOFCs. The crystal structure, oxygen non-stoichiometry, electrical conductivity, electrochemical performance, stability in air and  $\text{CO}_2$  tolerance performance were systematically investigated. The average bonding energy (ABE) and the increased critical radius ( $r_c$ ) were applied to discuss the influence of cation deficiency on ORR electro-catalytic activity. A proper cation deficiency may provide a simple and available strategy to develop highly active and stable perovskite materials for intermediate-to-low temperature SOFCs.

## 2. Experimental

### 2.1. Sample preparation

Solid-state reaction route was used to synthesize  $\text{SrCo}_{0.8}\text{Nb}_{0.1}\text{Ta}_{0.1}\text{O}_{3-\delta}$  (S100CNT),  $\text{Sr}_{0.95}\text{Co}_{0.8}\text{Nb}_{0.1}\text{Ta}_{0.1}\text{O}_{3-\delta}$  (S095CNT) and  $\text{Sr}_{0.90}\text{Co}_{0.8}\text{Nb}_{0.1}\text{Ta}_{0.1}\text{O}_{3-\delta}$  (S090CNT) powders. Stoichiometric amounts of  $\text{SrCO}_3$  (99.9%),  $\text{Co}_3\text{O}_4$  (99.9%),  $\text{Nb}_2\text{O}_5$  (99.9%) and  $\text{Ta}_2\text{O}_5$  (99.9%) were mixed and milled using ethanol as solvent media. After ethanol evaporation in the oven, the powders were calcined at  $1150^\circ\text{C}$  in air for 10 h. An additional milling and calcination was carried out to ensure complete mixing and reaction. The resultant aggregates were then ground again to obtain the cathode powders. Then, the powders were pressed into bars ( $5 \times 5 \times 60 \text{ mm}^3$ ) under sustained pressure at 200 MPa. The obtained bar samples were sintered at  $1200^\circ\text{C}$  for 5 h in air for conductivity test. The preparation of BSCF powder was identical to that of SDC powder below. Stoichiometric amounts of nitrates and glycine were dissolved in deionized water. After heating and drying in  $250^\circ\text{C}$  oven, a brown precursor powder was obtained, and then calcined at  $950^\circ\text{C}$  for 4 h in air to obtain BSCF powder.

The  $\text{Sm}_{0.2}\text{Ce}_{0.8}\text{O}_{1.9}$  (SDC) powders for electrolyte were synthesized using a glycine – nitrate process (GNP). Stoichiometric amounts of  $\text{Ce}(\text{NO}_3)_3 \cdot 6\text{H}_2\text{O}$  (99.5%),  $\text{Sm}(\text{NO}_3)_3 \cdot 6\text{H}_2\text{O}$  (99.5%) and glycine were dissolved in deionized water. After heating and drying in  $250^\circ\text{C}$  oven, a brown precursor powder was obtained. The precursor powders were then calcined at  $800^\circ\text{C}$  for 4 h in air to form SDC powders. The SDC powders were ground and dry-pressed into pellets ( $\phi 15 \text{ mm}$ ) under 200 MPa. Then, dense SDC substrates were prepared by sintering at  $1400^\circ\text{C}$  for 4 h in air.

### 2.2. Cell fabrication

Symmetric cells with S095CNT | SDC | S095CNT and S100CNT | SDC | S100CNT were fabricated for electrochemical impedance spectroscopy (EIS) measurements. The cathode slurry, which was prepared by mixing cathode powders with ethyl cellulose in terpineol, was printed on both sides of SDC disks and subsequently calcined at  $1000^\circ\text{C}$  for 2 h in stagnant air. Symmetric cell of BSCF | SDC | BSCF was fabricated with a similar process using SDC pellets as electrolyte and BSCF as symmetrical electrodes. The electrode slurry of BSCF was printed on both sides of SDC electrolyte and subsequently calcined at  $950^\circ\text{C}$  for 2 h in air. A thin layer of silver paste was painted onto the electrode surface

and dried at  $700^\circ\text{C}$  for 30 min for current collection.

The electrolyte-supported single cells S095CNT | SDC | NiO + SDC and S100CNT | SDC | NiO + SDC were fabricated for *I*-*V* tests. The well-mixed NiO + SDC (60:40 by weight ratio) anode powders and 10 wt% starch were milled and then screen-printed on the electrolyte substrate and sintered at  $1200^\circ\text{C}$  for 2 h. Subsequently, cathode slurries were screen-printed on the other side of the electrolyte. The completed triple-layered cells were finally fired at  $1000^\circ\text{C}$  for 2 h in air. The anode-supported single cell S095CNT | SDC | NiO + SDC was also fabricated using co-sintering process. NiO, SDC and starch powders were mixed in a weight ratio of 6:4:1 and pre-pressed, and then SDC powders were added and pressed. The bi-layer was sintered at  $1400^\circ\text{C}$  for 4 h in air. Cathode slurry was screen-printed on the electrolyte surface and sintered at  $1000^\circ\text{C}$  for 2 h.

### 2.3. Characterization

The X-ray diffraction (XRD) analyses were performed at room temperature using Shimadzu X-ray Diffractometer (Shimadzu, XRD-6100) with Cu K $\alpha$  radiation (voltage 40 KV and current 30 mA) with a step rate of  $0.02^\circ\text{s}^{-1}$ . Rietveld refinement was carried out to determine the crystal structure by using GSAS software. The oxygen non-stoichiometry at room temperature were determined by iodometric titration as described in our previous work [30]. The microscopic features of the electrodes were observed by field-emission scanning electron microscopy (FESEM, Quant 250FEG). A four-terminal DC method was used to measure the electrical conductivity of bar samples in air at  $100$ – $800^\circ\text{C}$  with an interval of  $50^\circ\text{C}$ . The electrical conductivity relaxation (ECR) measurement was used to determine the surface exchange coefficient ( $k^*$ ) and bulk diffusion coefficient ( $D^*$ ) over the cathode materials. The oxygen partial pressure was suddenly changed from 0.10 to 0.01 atm. The variation of conductivity was recorded continuously with relaxation time until it finally reached equilibrium again.

Electrochemical impedance spectroscopy (EIS) measurements were performed on symmetric cells with electrochemical workstation (CHI 660D) under open circuit voltage (OCV) conditions. The applied frequency of electrical perturbation was ranged from 0.1 to 100 KHz with amplitude of 10 mV. The partial pressure of oxygen (0.01, 0.21, 0.50, 1.00 atm) was controlled by adjusting the ratio of oxygen and nitrogen. The EIS experimental data were fitted using the ZView Software. The symmetrical cell (S095CNT | SDC | S095CNT) was test in air at  $600^\circ\text{C}$  for 100 h to evaluate the stability of S095CNT cathode. Additionally, the symmetrical cell was tested at  $600^\circ\text{C}$  in air by introducing different concentration of  $\text{CO}_2$  (1%, 5% and 10%) to study the  $\text{CO}_2$  tolerance of the cathode.

The *I*-*V* tests of single cells were measured with a home-made fuel cell testing system. The prepared single cell was sealed in a ceramic tube with high temperature sealant and then dried at room temperature for 12 h. Humidified hydrogen was applied as fuel at a flow rate of  $100 \text{ ml min}^{-1}$ , and ambient air was used as the oxidant gas in the cathode side.

## 3. Results and discussion

### 3.1. Crystal structure

The phase formation of  $\text{Sr}_x\text{Co}_{0.8}\text{Nb}_{0.1}\text{Ta}_{0.1}\text{O}_{3-\delta}$  ( $x = 0.90, 0.95, 1.00$ ) were confirmed by X-ray diffraction (XRD) analyses in Fig. 1. The diffraction peak pattern of the S100CNT and S095CNT are identified as cubic perovskite phase (JCPDS 70–3971). However, a second phase, CoO was observed on the XRD patterns of S090CNT sample. Therefore, the Sr deficiency limit of in  $\text{S}_x\text{CNT}$  is hoped to be at approximately 5 mol% to void a phase decomposition.

Rietveld refinement of the S095CNT and S100CNT were performed using the general structure analysis system (GSAS) program and the

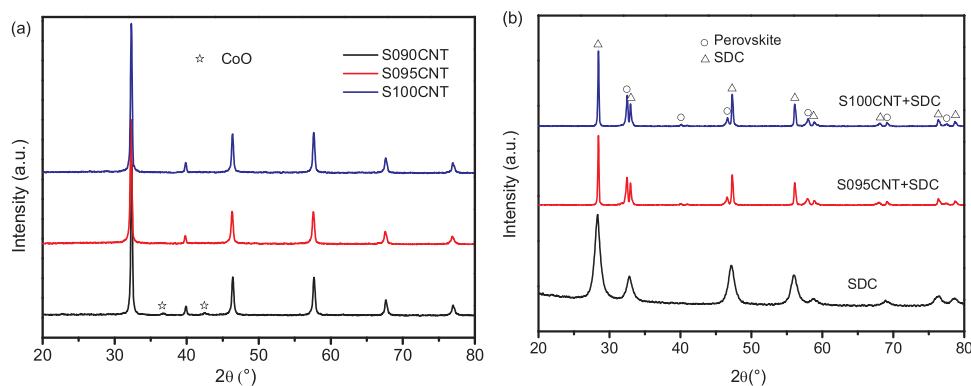


**Fig. 1.** (a) XRD patterns for  $\text{Sr}_x\text{Co}_{0.8}\text{Nb}_{0.1}\text{Ta}_{0.1}\text{O}_{3-\delta}$  ( $x = 0.90, 0.95, 1.00$ ) sintered at 1150 °C for 10 h and (b) S095CNT-SDC and S100CNT-SDC mixed powders (1:1 wt ratio) after calcining at 1000 °C for 4 h.

results are shown in Fig. S1. S100CNT could be indexed to a cubic structure with a space group symmetry  $Pm-3m$  and a lattice constant of  $a = 3.921 \text{ \AA}$  and  $v = 60.280 \text{ \AA}^3$ , while the lattice parameter of S095CNT shows larger values of  $a = 3.944 \text{ \AA}$  and  $v = 61.348 \text{ \AA}^3$  with the space group  $Pm-3m$  symmetry. Furthermore, chemical compatibility between S095CNT, S100CNT and SDC has also been investigated by mixing the composite powders at 1:1 wt ratio and firing at 1000 °C for 4 h in air, and XRD results are shown in Fig. 1(b). It is demonstrated that all peaks have been labelled as perovskite phase and SDC patterns and no other phases are observed, indicating that S095CNT and S100CNT have a good chemical compatibility with SDC electrolyte. In order to analysis the effect of cation deficiency on oxygen non-stoichiometry, electrical and electrochemical performance of SCNT perovskites with pure phase, S095CNT and S100CNT were taken as samples in the following investigations.

### 3.2. Oxygen non-stoichiometry

Oxygen non-stoichiometry of the S095CNT and S100CNT oxides in air were characterized by iodometric titration method and thermogravimetric analysis at various temperatures [31,32]. A similar variation trend of weight loss can be observed for S095CNT and S100CNT shown in Fig. 2(a). When the temperature is below 275 °C, the slow weight loss of TGA curves may be due to the loss of adsorbed water and other gases. While the curves display a sharp weight loss at 275 °C, which is attribute to the release of lattice oxygen. A similar phenomenon has also been observed in the case of  $\text{Pr}_{1-x}\text{BaCo}_2\text{O}_{5+\delta}$  [33]. The curves show a mass weight loss that is mainly due to the reduction of  $\text{Co}^{4+}$  to  $\text{Co}^{3+}$ , which is accompanied by lattice oxygen release to form oxygen vacancies [34], according to Eq. 1. The weight loss equilibrium region was observed at 275–350 °C, which might be the redox equilibrium reaction between  $\text{Co}^{3+} \rightarrow \text{Co}^{4+}$  and  $\text{Co}^{3+} \rightarrow \text{Co}^{2+}$ , and similar with the case of  $\text{Fe}^{3+} \rightarrow \text{Fe}^{4+}$  and  $\text{Fe}^{3+} \rightarrow \text{Fe}^{2+}$  in  $\text{La}_{1-x}\text{Sr}_x\text{FeO}_{3-\delta}$  oxide

[35].

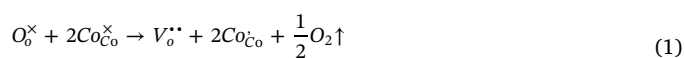


Fig. 2(b) displays the thermal evolution of oxygen non-stoichiometry of S095CNT and S100CNT at 50–800 °C. The S095CNT oxide shows higher oxygen vacancy concentration than the stoichiometric S100CNT in the whole measured temperature range. Combined with the results of crystal structure change displays in Fig. 1, it can be deduced that the Sr-deficiency in SCNT perovskite causes a small lattice expansion, and thus an additional oxygen vacancy. It is worth noting that the additional oxygen vacancies are beneficial for promotion on ORR activity of cathode materials.

### 3.3. Electrical conductivity

Temperature dependence of electrical conductivity of S095CNT and S100CNT samples in air are shown in Fig. 3(a). Since the electronic conductivity is usually at least two orders of magnitude higher than the ionic conductivity, and as such, the measured electrical conductivity can be regarded as the electronic conductivity. The electrical conductivity increased with elevated temperature until 400 °C, and the Arrhenius plots presents a linear relationship up to a transition temperature in Fig. 3(b), corresponding to the small polaron hopping mechanism, in which the electron holes act as the charge carriers [36]. However, the electrical conductivity decreases over a transition temperature. This is resulted from the release of lattice oxygen from these perovskite oxides at high temperature [37], which will lead to the partial annihilation of electronic holes ( $h^\bullet$ ) and thus the decreased electronic conductivity, as described by Eq. (2).



The maximum conductivity for S100CNT is about  $74 \text{ S cm}^{-1}$  but the

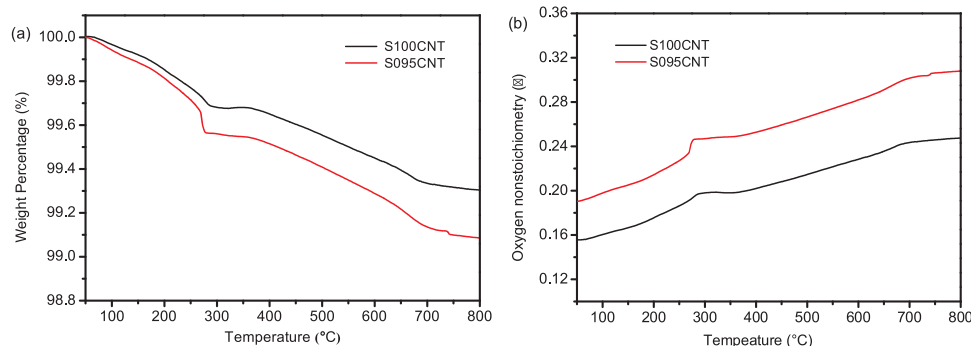


**Fig. 2.** Mass and oxygen non-stoichiometry change of S095CNT and S100CNT as a function of temperature in air.

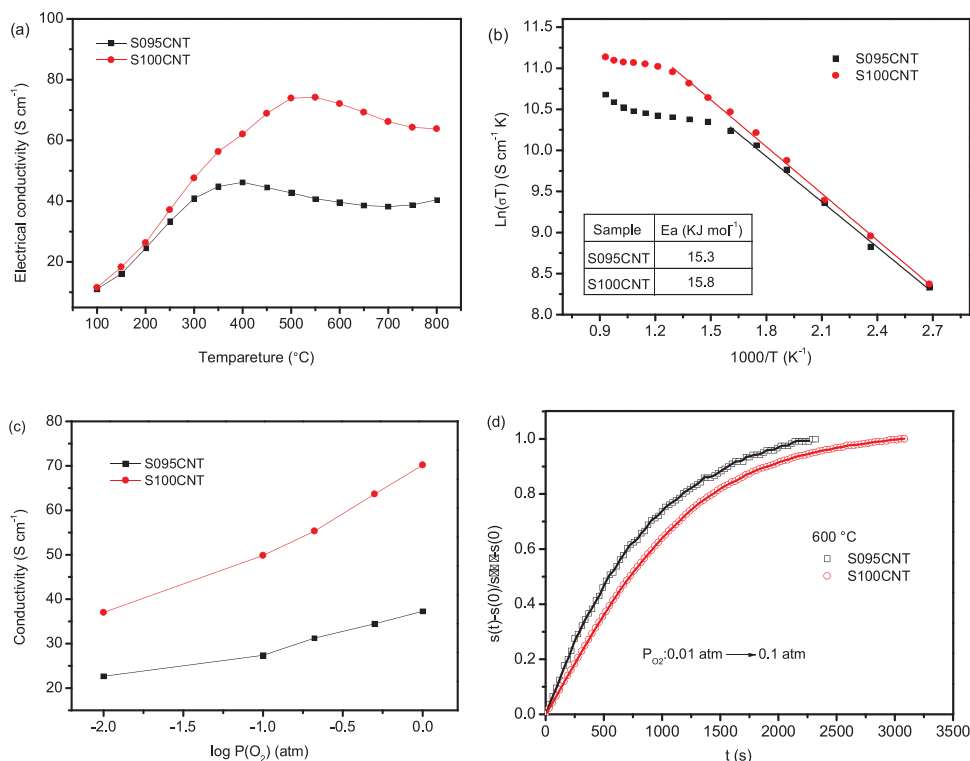


**Fig. 3.** (a) Temperature dependence of electrical conductivity of S095CNT and S100CNT samples in air, (b) Corresponding Arrhenius plots of the samples, (c) Electrical conductivity of S095CNT and S100CNT at different  $p(\text{O}_2)$  (atm) at 600 °C, and (d) Normalized conductivity data of S095CNT and S100CNT at a sudden change with  $p(\text{O}_2)$  from 0.01 to 0.1 atm at 600 °C by electrical conductivity relaxation technique.

highest conductivity for S095CNT is only 46 S cm<sup>-1</sup>. Similar results were found in the case of (Ba<sub>0.5</sub>Sr<sub>0.5</sub>)<sub>1-x</sub>Co<sub>0.8</sub>Fe<sub>0.2</sub>O<sub>3-δ</sub> ( $x = 0.00$ – $0.15$ ) [38]. Furthermore, the activation energy of S095CNT and S100CNT samples were calculated according to the Arrhenius equation,

$$\sigma = \frac{A}{T} \exp\left(\frac{-E_a}{kT}\right) \quad (3)$$

where  $T$  is the absolute temperature,  $A$  is a pre-exponential factor,  $E_a$  is the activation energy, and  $k$  represents the Boltzmann constant. Here, the  $E_a$  values, which are calculated from the slope of the Arrhenius plot, are 15.3 and 15.8 KJ mol<sup>-1</sup> for S095CNT and S100CNT oxides, respectively, and comparable to those mixed ionic and electronic conductors, such as Ba<sub>1-x</sub>La<sub>x</sub>FeO<sub>3-δ</sub> (18.6–31.2 kJ mol<sup>-1</sup>) [39], BaCo<sub>0.6</sub>Fe<sub>0.3</sub>Sn<sub>0.1</sub>O<sub>3-δ</sub> (34.6 ± 0.4 kJ mol<sup>-1</sup>) [40,41].

The intrinsic properties, such as the bulk diffusion and surface exchange kinetics, are closely related to the cathode performance [42,43]. Here, electrical conductivity relaxation (ECR) technique is employed to determine surface exchange coefficient ( $k^*$ ) and bulk diffusion coefficient ( $D^*$ ) of the perovskite oxides at an abrupt change in the oxygen partial pressure of the surrounding atmosphere. The electrical conductivity of S095CNT and S100CNT increases with increasing partial oxygen pressure at 600 °C (Fig. 3(c)), indicating that both of them are typical  $p$ -type conductor. Moreover, the normalized conductivity curves at 600 °C as a function of the elapsed time for S095CNT and S100CNT was given in Fig. 3(d). The electrical conductivity relation curves were fitted using the least square method [44]. The  $k^*$  and  $D^*$  values are shown on Table 1. The  $k^*$  and  $D^*$  values in this work is of the same order of magnitude with those of BCFY cathode [45], and much larger than those other state-of-the-art cathode materials, such as LSCF and BSCF [46,47]. Both  $k^*$  and  $D^*$  for S095CNT are higher than those of S100CNT, indicating faster oxygen surface adsorption/desorption and bulk charge diffusion kinetics for the former.

### 3.4. ORR activity

The electrochemical impedance spectra of S095CNT and S100CNT cathodes were investigated at 500–650 °C in air as shown in Fig. 4(a)

**Table 1**

Room-temperature lattice parameters and oxygen concentration, surface exchange coefficient ( $k^*$ ), the bulk diffusion coefficient ( $D^*$ ),  $R_p$  and peak power density (PPD) at 600 °C for S095CNT and S100CNT.

Sample	$a = b = c$ (Å)	$\delta$	$k^*$ (cm s <sup>-1</sup> )	$D^*$ (cm <sup>2</sup> s <sup>-1</sup> )	$R_p$ (Ω cm <sup>2</sup> )	PPD <sup>*</sup> (mW cm <sup>-2</sup> )
S095CNT	3.944	0.196	$2.45 \times 10^{-3}$	$8.74 \times 10^{-4}$	0.12	281
S100CNT	3.921	0.175	$1.71 \times 10^{-3}$	$4.17 \times 10^{-4}$	0.17	162

\* The single cell is an electrolyte-supported cell with electrolyte thickness of 220 μm.

and (b). The polarization resistance ( $R_p$ ) can be roughly calculated from the intercept of  $Z'$  axis, and the corresponding values are 0.07, 0.12, 0.24, 0.58 Ω cm<sup>2</sup> for S095CNT, and 0.11, 0.17, 0.36, 0.87 Ω cm<sup>2</sup> at 650, 600, 550 and 500 °C for S100CNT shown in Fig. 4(c), which is substantially lower than that reported for other Co-based perovskite cathodes even at higher temperature, such as SrCo<sub>0.9</sub>Ta<sub>0.1</sub>O<sub>3-δ</sub> (0.21 Ω cm<sup>2</sup> at 700 °C) [48], SrCo<sub>0.9</sub>Ti<sub>0.1</sub>O<sub>3-δ</sub> (0.17 Ω cm<sup>2</sup> at 700 °C) [49], SrCo<sub>0.7</sub>Ta<sub>0.1</sub>Fe<sub>0.2</sub>O<sub>3-δ</sub> (0.89 Ω cm<sup>2</sup> at 600 °C) [50], SrCo<sub>0.7</sub>Nb<sub>0.1</sub>Fe<sub>0.2</sub>O<sub>3-δ</sub> (0.64 Ω cm<sup>2</sup> at 600 °C) [30], etc.

Notably, S095CNT shows a lower polarization resistance (Fig. 4(c)) and activation energy ( $E_a$ ) than that of S100CNT (Fig. 4(d)). A lower activation energy means a lower chemical barrier for oxygen reduction, subsequently a higher electro-catalytic activity at reduced temperature [51]. These results indicate that the cation deficiency in the perovskite structure could lead to more surface defect sites to accept molecular oxygen and enhanced diffusivity of oxygen ions inside the bulk, which synergistically promoted the ORR performance of SCNT cathode.

Both the critical radius ( $r_c$ ) and the average bonding energy (ABE) of metal-oxygen have positively impact on the O<sup>2-</sup> transport in perovskite structure [52,53]. The critical radius is the narrowest position for oxygen ion transfer, formed by two A-site cations and one B-site cation, as shown in Fig. S2 (a). The critical radius can be given by Eq 4 [54],

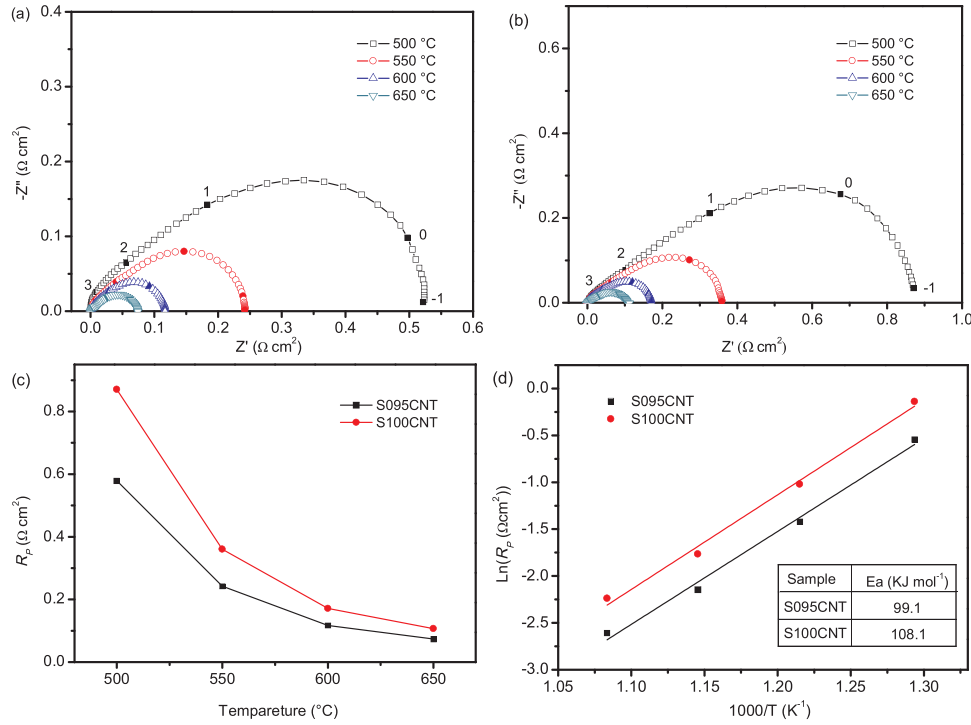


**Fig. 4.** Electrochemical impedance spectra of (a) S095CNT and (b) S100CNT at 500–650 °C, (c) polarization resistance  $R_p$  as a function of temperature and (d) corresponding Arrhenius plots of S095CNT and S100CNT cathode in air.

**Table 2**

Average bonding energy of metal-oxygen for S095CNT and S100CNT samples.

Sample	< A–O > (KJ mol <sup>-1</sup> )	< B–O > (KJ mol <sup>-1</sup> )			< ABE > (KJ mol <sup>-1</sup> )
		< Co–O >	< Nb–O >	< Ta–O >	
S095CNT	–79.681	–140.688	–38.333	–40.504	–299.207
S100CNT	–83.875	–140.688	–38.333	–40.504	–303.400

$$r_c = \frac{-r_A^2 + \frac{3}{4}(a^2) - \sqrt{2}(a)(r_B) + r_B^2}{2r_A + \sqrt{2}a - 2r_B} \quad (4)$$

For S095CNT and S100CNT samples,  $r_A = r_{Sr^{2+}}$  and  $r_B = 0.8[xr_{Co^{3+}} + (1-x)r_{Co^{2+}}] + 0.1r_{Nb^{5+}} + 0.1r_{Ta^{5+}}$ , the critical radius of S095CNT and S100CNT cathodes was calculated and plotted in Fig. S2 (b).

The average metal (A,B)–oxygen bond energy within the perovskite lattice (< ABE >), the average A(A)–O (< A–O >) and B(B',B'')–O (< B–O >) bond energies for a cation stoichiometric  $A_{1-x}A'_xB_{1-y-z}B''_zO_3$  and for A-site deficient  $(A_{1-x}A'_x)_wB_{1-y-z}B''_zO_3$  compositions were estimated as follows [55],

$$< ABE > = < A-O > + < B-O > \quad (5)$$

$$< A-O > = \Delta(A-O) + \Delta(A'-O) \quad (6)$$

$$< B-O > = \Delta(B-O) + \Delta(B'-O) + \Delta(B''-O) \quad (7)$$

$$\Delta(A-O) = \frac{x_A}{CN_A \times m} \times (\Delta H_{AmOn} - m \times \Delta H_A - \frac{n}{2} \times D_{O_2}) \quad (8)$$

$$\Delta(A-O) = \frac{x_A \cdot w}{CN_A \times m} \times (\Delta H_{AmOn} - m \times \Delta H_A - \frac{n}{2} \times D_{O_2}) \quad (9)$$

(in the case of A-site deficiency)

$$\Delta(B-O) = \frac{y_B}{CN_B \times m} \times (\Delta H_{BmOn} - m \times \Delta H_B - \frac{n}{2} \times D_{O_2}) \quad (10)$$

where  $x_A$  and  $y_B$  are the molar fraction of A and B metals;  $w$  is the fraction of A-site cations in A-site deficient compositions

$(A_{1-x}A'_x)_wB_{1-y-z}B''_zO_3$  ( $w < 1$ );  $\Delta H_{A(B)mOn}$  and  $\Delta H_{A(B)}$  are the enthalpy of formation of one mole of  $A(B)mOn$  oxides and the sublimation energy of  $A(B)$  metal at 25 °C,  $CN_{A(B)}$  is the coordination number of cations on the A and B sites, and  $D_{O_2}$  is the dissociation energy of  $O_2$  (500.2 KJ mol<sup>-1</sup>). The equations applied to A', B' and B'' are similar to A and B. For S095CNT and S100CNT samples,  $\Delta H_{Sr} = 164.4 \text{ KJ mol}^{-1}$ ,  $\Delta H_{Co} = 424.7 \text{ KJ mol}^{-1}$ ,  $\Delta H_{Nb} = 721.05 \text{ KJ mol}^{-1}$ ,  $\Delta H_{Ta} = 782.0 \text{ KJ mol}^{-1}$ ,  $\Delta H_{SrO} = -592.0 \text{ KJ mol}^{-1}$ ,  $\Delta H_{Co3O4} = -891.0 \text{ KJ mol}^{-1}$ ,  $\Delta H_{Nb2O5} = -1897.72 \text{ KJ mol}^{-1}$ ,  $\Delta H_{Ta2O5} = -2046.0 \text{ KJ mol}^{-1}$  and the calculate results as shown on Table 2.

It is obvious that the S095CNT display a higher  $r_c$  and lower ABE than that of S100CNT as displayed in Fig. S1 (b) and on Table 2. A large  $r_c$  and small ABE values are favorable for the migration of oxygen ions in perovskite lattice, resulting in a decrease of activation energy for  $O^{2-}$  transport. Thus, the S095CNT with larger  $r_c$  and smaller ABE may be more beneficial as a cathode of SOFC for oxygen reduction reaction at evaluated temperature.

To get more insight into intrinsic ORR processes of the cathode, the S095CNT | SDC | S095CNT and S100CNT | SDC | S100CNT symmetric cells were exposed in different oxygen pressure at 550 °C, and the electrochemical impedance spectra were recorded on Fig. 5(a) and (b). And the data were fitted using an equivalent circuit  $LR_0(R_1Q_1)(R_2Q_2)$ , where  $L$  was the inductance caused by the electrical equipment and lead wire, and  $R_0$  was mainly related to the ohmic resistance of the electrolyte. The high frequency arcs related resistance  $R_1$  was associated with the charge-transfer process which included the electron and ion transfer process. The low frequency arcs about  $R_2$  was attributed to mass transfer process [56,57]. In general, the relationship between the polarization resistance ( $R_p$ ) and the oxygen partial pressure ( $p_{O_2}$ ) is shown as follows,

$$R_p = K(p_{O_2})^{-n} \quad (11)$$

where  $k$  is a constant, and  $n$  is the parameter related to the rate-determining step [58].

As shown in Fig. 5(c) and (d), the  $n$  value for low frequency is 0.44 and 0.46 for S095CNT and S100CNT. Thus, the low frequency arc ( $R_2$ )

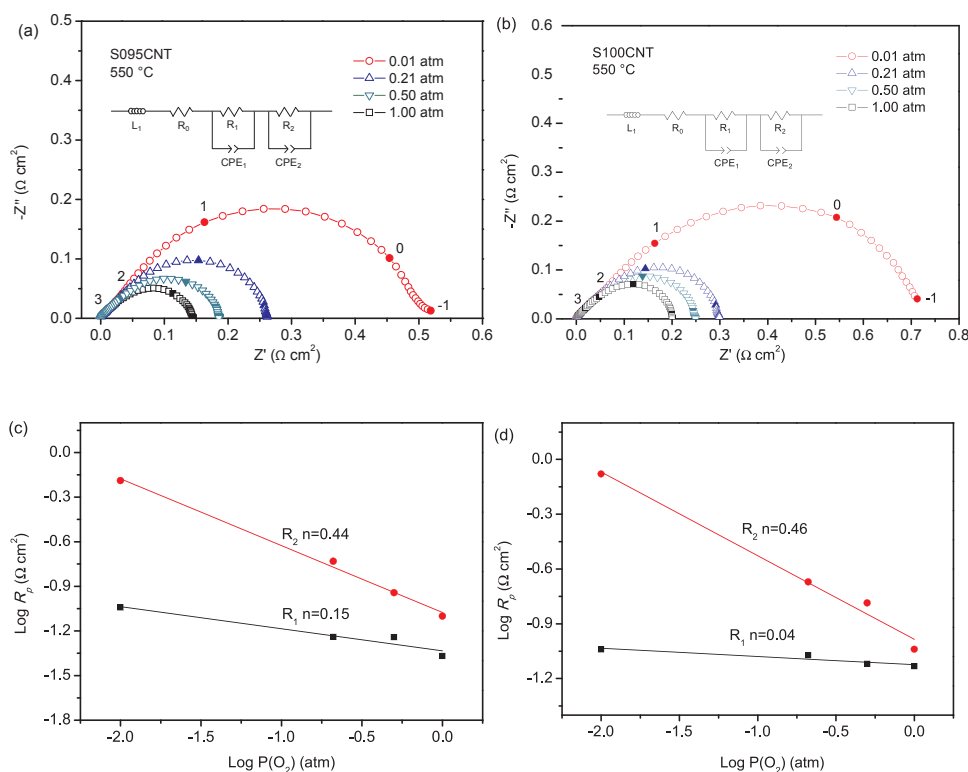


**Fig. 5.** Impedance spectra of (a) S095CNT and (b) S100CNT cathodes measured at 550 °C under various oxygen partial pressures, the logarithm of the frequency decade is indicated, and polarization resistance of (c) S095CNT, (d) S100CNT cathodes at high frequency ( $R_1$ ) and low frequency ( $R_2$ ) as a function of logarithm of oxygen partial pressure.

is related to the oxygen adsorption-desorption process with  $n = 1/2$  (Eq. (12)). The impedance response of the high frequency ( $R_1$ ) is found to have a dependence about 0.15 on the oxygen partial pressure for S095CNT and about 0.04 for S100CNT, which is close to the theoretical value  $n = 1/8$  (Eq. (13)) and  $n = 0$  (Eq. (14)). Thus, the high frequency arc is related to the oxygen ion reduction process at TPBs for S095CNT cathode, and oxygen ion transfer within the bulk electrode and/or from electrode to SDC electrolyte for S100CNT.

$$n = \frac{1}{2}, O_{2,ads} \rightleftharpoons 2O_{TPB} \quad (12)$$

$$n = \frac{1}{8}, O_{TPB}^- + e^- \rightleftharpoons O_{TPB}^{2-} \quad (13)$$

$$n = 0, O_{TPB}^{2-} + V_O^{\bullet\bullet} \rightleftharpoons O_O^{\times} \quad (14)$$

### 3.5. Single cell performance

I-V and I-P curves of the electrolyte-supported single cells S095CNT | SDC | Ni + SDC and S100CNT | SDC | Ni + SDC are presented in Fig. 6(a) and (b). The maximum power density reaches 223 mW cm<sup>-2</sup> at 650 °C for the single cell with S100CNT cathode, whereas a higher maximum power density of 332 mW cm<sup>-2</sup> is obtained for that with S095CNT cathode, which is higher than those of SrCo<sub>0.7</sub>Nb<sub>0.1</sub>Fe<sub>0.2</sub>O<sub>3-δ</sub> (120 mW cm<sup>-2</sup> at 650 °C) and Sr<sub>0.95</sub>Co<sub>0.7</sub>Nb<sub>0.1</sub>Fe<sub>0.2</sub>O<sub>3-δ</sub> (150 mW cm<sup>-2</sup> at 650 °C [30]) with similar structure. As mentioned above, the A-site Sr-deficient S095CNT cathode demonstrated a lower ABE and a higher  $r_c$ , which are beneficial for the migration of oxygen ions. Hence, the S095CNT displayed higher ORR electro-catalytic activity, and thereby promoted cell power density. The morphology of the single cells after electrochemical measurement is shown in Fig. 6 (c) and (d). The thickness of the SDC electrolyte is approximately 220 μm. The anode is porous and has uniformly distributed particles with an average size about 1–2 μm. Both cathodes exhibit uniform porosity, indicating excellent gas diffusion. The S095CNT cathode attaches firmly to the electrolyte with nice thermal compatibility between the cathode and

electrolyte. Hence, the S095CNT displays higher ORR activity as well as better thermal compatibility, and thereby higher cell power density. Moreover, the anode-supported single cell performance with S095CNT cathode was investigated (Figure S3). And the maximum power density is 475 mW cm<sup>-2</sup> at 650 °C. Considering the thickness of SDC electrolyte of this cell is about 60 μm, improved power density of the cell could be obtained if the electrolyte thickness could be further reduced.

### 3.6. Stability test

Finally, we studied the short-term stability of S095CNT cathode with a symmetrical cell S095CNT | SDC | S095CNT at 600 °C in air for 100 h, as show in Fig. 7. The  $R_p$  of S095CNT cathode was stable at ~0.12 Ω cm<sup>2</sup> with an increasing rate of ~4.90 × 10<sup>-4</sup> Ω cm<sup>2</sup>/h during the overall test period. Moreover, the grain size of S095CNT cathode after 100 h stability test was similar as that of the pristine S095CNT cathode, as shown from the SEM images inserted in Fig. 7. The slight fluctuation of the  $R_p$  may be associated with decreased of the silver current collector during this period, leading to the degradation of the overall cathode performance [59]. As one can see that the impedance of the S095CNT electrode remained relatively constant in 1% CO<sub>2</sub> containing atmospheres during the testing period, similar to that in air, indicating that S095CNT has a good CO<sub>2</sub> tolerance in low concentration CO<sub>2</sub> containing atmospheres. The S095CNT cathode demonstrated a highly stability, indicating that S095CNT holds great promise as a potential ORR electro-catalyst for application in IT-SOFCs.

CO<sub>2</sub> tolerance is another important requirement for these perovskite cathodes containing alkaline earth metals because carbonates are easily formed in the presence of CO<sub>2</sub>, in turn, leading to deteriorate the cathode performance [60–62]. To investigate the CO<sub>2</sub> tolerance of the SCNT perovskite cathode, the  $R_p$  values of S095CNT, S100CNT and BSCF cathodes were tested in air containing various concentrations of CO<sub>2</sub> at 600 °C (Fig. 8(a)). Compared to the state-of-the-art BSCF cathode, the S095CNT, S100CNT cathodes show negligible increase in their  $R_p$  values, especially in air containing 1% and 5% CO<sub>2</sub>. As shown in Fig. 8(b), the relative increase ratio of  $R_p$  is 3–6 times higher for BSCF

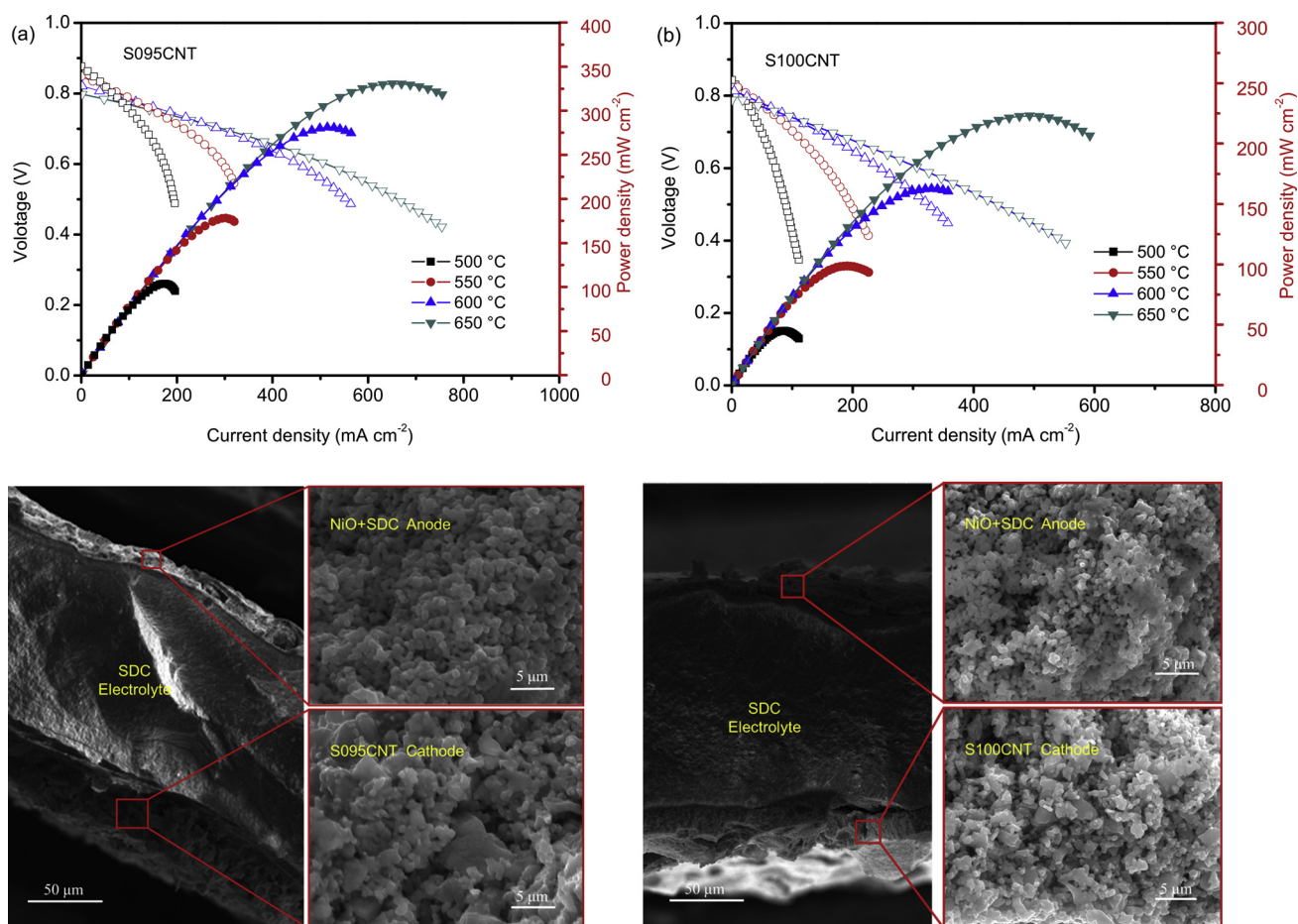


**Fig. 6.** I–V and I–P curves for electrolyte-supported single cells with dry  $H_2$  as fuel and ambient air as oxidant at 500–650 °C: (a) S095CNT | SDC | NiO + SDC and (b) S100CNT | SDC | NiO + SDC. And SEM images of electrolyte-supported single cells: (c) S095CNT | SDC | NiO + SDC, (d) S100CNT | SDC | NiO + SDC.

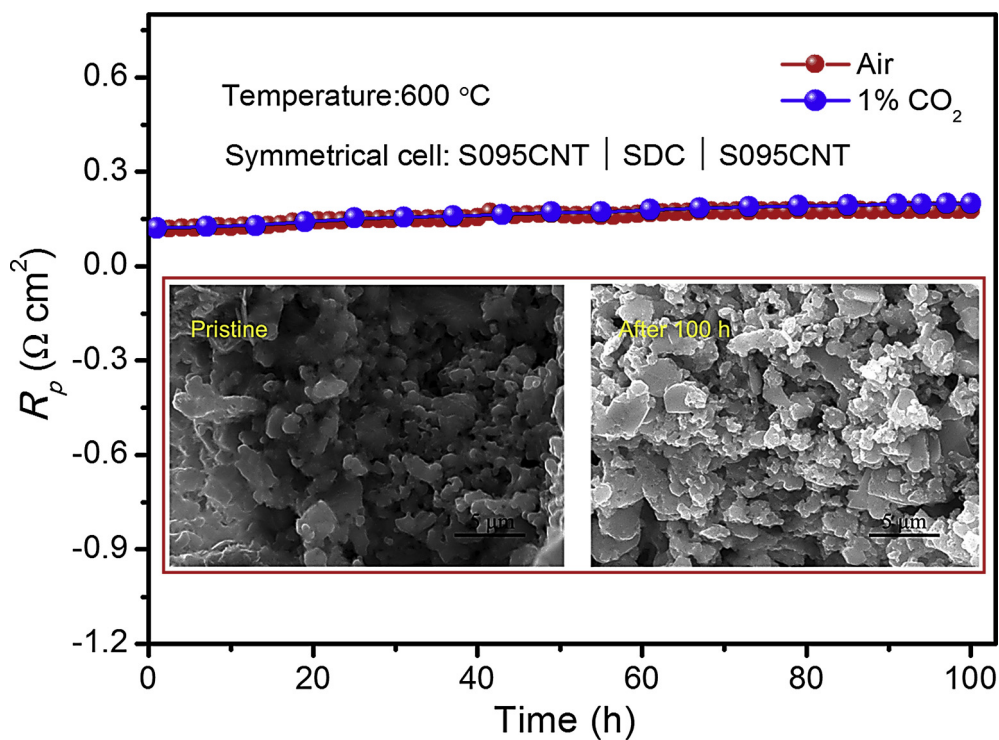


**Fig. 7.** Polarization resistance of S095CNT cathode in a symmetrical cell at 600 °C in air and 1%  $CO_2$  containing atmospheres for 100 h, and the insets are the SEM images for the pristine and tested S095CNT cathode in air.

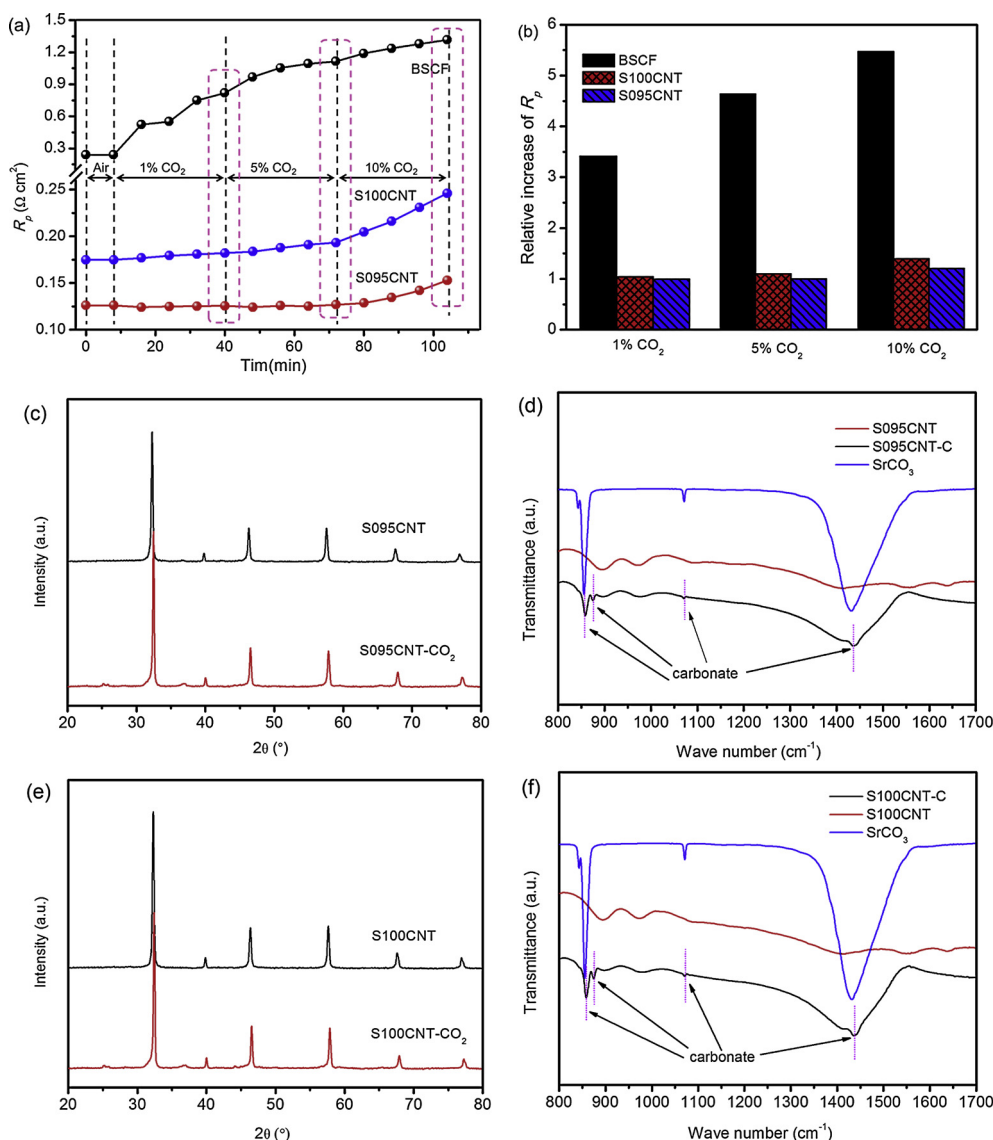


**Fig. 8.** Time-dependent  $R_p$  values of S095CNT, S100CNT and BSCF cathodes treated in various  $\text{CO}_2$  concentrations in air (1%, 5% and 10%) at  $600^\circ\text{C}$ , (b) relative increases of  $R_p$  of S095CNT, S100CNT and BSCF after  $\sim 30$  min in air containing  $\text{CO}_2$  at various concentration. The XRD patterns of (c) fresh S095CNT and S095CNT after  $\text{CO}_2$  treatment, (e) fresh S100CNT and S100CNT after  $\text{CO}_2$  treatment after  $\text{CO}_2$  treatment for 2 h at  $600^\circ\text{C}$ ; FT-IR spectra of (d) fresh S095CNT and S095CNT after  $\text{CO}_2$  treatment, (f) fresh S100CNT and S100CNT after  $\text{CO}_2$  treatment for 2 h at  $600^\circ\text{C}$ .

after an exposure in air with various concentration of  $\text{CO}_2$  compared with the blank BSCF, indicating a severe  $\text{CO}_2$  contamination for the state-of-the-art BSCF cathode. However, the relative increase ratio of  $R_p$  is much lower for S100CNT (1–1.4 times) and S095CNT (1–1.2 times) cathodes after a treatment in air with 1%–10%  $\text{CO}_2$ . In the operation condition, the reaction between cathode and  $\text{CO}_2$  is regarded as a chemical reaction between an acid ( $\text{CO}_2$ ) and a base (cathode) based on the Lewis acid-base theory in which an acid is regarded as any compound which, in a chemical reaction, is able to attach itself to an unshared pair of electrons in another molecule [63]. The acidity order of the cations in SCNT and BSCF is  $\text{Nb}^{5+} > \text{Ta}^{5+} > \text{Co}^{4+} > \text{Co}^{3+} > \text{Fe}^{3+} > \text{Sc}^{3+} > \text{Co}^{2+} > \text{Fe}^{2+} > \text{Sr}^{2+} > \text{Ba}^{2+}$  [64]. Thus, the S095CNT and S100CNT perovskites would show a lower basicity due to the doping of relatively high acidity cations ( $\text{Nb}^{5+}$  and  $\text{Ta}^{5+}$ ) [62,65]. Consequently, the S095CNT and S100CNT display a superior  $\text{CO}_2$  tolerance than that of BSCF. Additionally, a competitive relation normally exists between  $\text{O}_2$  and  $\text{CO}_2$  competitive adsorption of surface active sites. The S095CNT shows a lower  $\langle \text{ABE} \rangle$  value ( $-299 \text{ kJ mol}^{-1}$ ) relative to that of S100CNT ( $-303 \text{ kJ mol}^{-1}$ ), similar to the case of SNC0.95 with higher ORR

activity and  $\text{CO}_2$  tolerance, and shows a lower  $\langle \text{ABE} \rangle$  value of ( $-287 \text{ kJ mol}^{-1}$ ) than that of SNC ( $-291 \text{ kJ mol}^{-1}$ ) [22,66]. The ABE difference between S095CNT and SCNT is small since the cation deficiency in the perovskite is tiny. Smaller ABE values are favorable for the migration of oxygen ions in perovskite lattice, resulting in a decrease of activation energy for  $\text{O}^{2-}$  transport, thus higher ORR activity with lower  $R_p$  (Fig. 8a). And the  $\text{CO}_2$  tolerance of S095CNT and SCNT is much better than that of BSCF. And the  $\text{CO}_2$  tolerance difference between S095CNT and SCNT is tiny (Fig. 8b), suggesting that the introduction of a proper cation deficiency may not degrade the SCNT perovskite stability on anti- $\text{CO}_2$ .

To detect the possible carbonate yielding after  $\text{CO}_2$  contamination, these perovskite oxides were exposed under high purity  $\text{CO}_2$  at  $600^\circ\text{C}$  for 2 h. The XRD patterns and Fourier-transform infrared (FT-IR) spectra of S095CNT (Fig. 8c and d), S100CNT (Fig. 8e and f) and BSCF (Fig. S4) were performed. Compared to the BSCF cathode, the carbonates were not detected in S095CNT and S100CNT cathodes from the XRD results as shown in Fig. 8c and e. Considering the low sensitivity of XRD technique to detect trace substance, FT-IR spectroscopy was performed to index the carbonates on the  $\text{CO}_2$ -treated oxides. The results in

Fig. 8(d), (f) revealed that the vibrational peaks of  $\text{CO}_3^{2-}$  in all  $\text{CO}_2$ -treated cathodes, indicating that the carbonates did indeed form after a high purity 100%  $\text{CO}_2$  treatment at 600 °C.

#### 4. Conclusion

A-site cation deficiency in  $\text{Sr}_{0.95}\text{Co}_{0.8}\text{Nb}_{0.1}\text{Ta}_{0.1}\text{O}_{3-\delta}$  perovskite strongly affects the lattice structure, oxygen vacancies concentration, electrical conductivity and oxygen reduction electro-catalytic activity. The Sr-site deficient S095CNT demonstrated increasing lattice parameters, higher oxygen vacancies concentration relative to the stoichiometric S100CNT cathode thereby obtaining an increased  $r_c$  and decreased ABE. Consequently, the polarization resistance of S095CNT at 650 °C was  $0.07 \Omega \text{ cm}^2$ , lower than that of S100CNT. The peak power density of SDC electrolyte supported single cell is  $332 \text{ mW cm}^{-2}$  for S095CNT cathode and  $223 \text{ mW cm}^{-2}$  for S100CNT cathode, respectively. Furthermore, The S095CNT cathode demonstrated excellent electrochemical stability and  $\text{CO}_2$  tolerance at 600 °C, indicating that Sr-site deficient S095CNT perovskite is a promising cathode material for IT-SOFCs due to its superior ORR activity and stability.

#### Acknowledgements

The authors acknowledge the generous financial support from the National Natural Science Foundation of China (51872143, 51790492, 51472118), the Fundamental Research Funds for the Central Universities (30916011104), A Project Funded by the Priority Academic Program Development of Jiangsu Higher Education Institutions (PAPD) and Open Foundation of Key Laboratory of Advanced Micro & nano Materials and Technology in Jiangsu Province (No. 30917014106).

#### Appendix A. Supplementary data

Supplementary material related to this article can be found, in the online version, at doi:<https://doi.org/10.1016/j.apcatb.2018.10.075>.

#### References

- [1] S.C. Singhal, Advances in solid oxide fuel cell technology, *Solid State Ion.* 135 (2000) 305–313.
- [2] A.J. Jacobson, Materials for solid oxide fuel cells, *Chem. Mater.* 22 (2010) 660–674.
- [3] Steele, C.H. Brian, H. Angelika, Materials for fuel-cell technologies, *Nature* 414 (2001) 345–352.
- [4] S. Yu, S. He, H. Chen, L. Guo, Effect of calcination temperature on oxidation state of cobalt in calcium cobaltite and relevant performance as intermediate-temperature solid oxide fuel cell cathodes, *J. Power Sources* 280 (2015) 581–587.
- [5] Y. Zhu, W. Zhou, R. Ran, Y. Chen, Z. Shao, M. Liu, Promotion of oxygen reduction by exsolved silver nanoparticles on a perovskite scaffold for low-temperature solid oxide fuel cells, *Nano Lett.* 16 (2016) 512–518.
- [6] Y. Zhang, G. Yang, G. Chen, R. Ran, W. Zhou, Z. Shao, Evaluation of the  $\text{CO}_2$  poisoning effect on a highly active cathode  $\text{Sr}_{0.175}\text{Nb}_{0.025}\text{Co}_{0.8}\text{O}_{3-\delta}$  in the oxygen reduction reaction, *ACS Appl. Mater. Interfaces* 8 (2016) 3003–3011.
- [7] J.C. Ruiz-Morales, D. Marrero-López, J. Canales-Vázquez, J.T.S. Irvine, Symmetric and reversible solid oxide fuel cells, *RSC Adv.* 1 (2011) 1403–1414.
- [8] J.H. Kim, M. Cassidy, J.T.S. Irvine, J. Bae, Electrochemical investigation of composite cathodes with  $\text{SmBa}_{0.5}\text{Sr}_{0.5}\text{Co}_2\text{O}_{5+\delta}$  cathodes for intermediate temperature-operating solid oxide fuel cell, *Chem. Mater.* 22 (2010) 883–892.
- [9] Y. Zhu, J. Sunarso, W. Zhou, Z. Shao, Probing  $\text{CO}_2$  reaction mechanisms and effects on the  $\text{SrNb}_{0.1}\text{Co}_{0.9-x}\text{Fe}_x\text{O}_{3-\delta}$  cathodes for solid oxide fuel cells, *Appl. Catal. B* (2015) 172–173 52–57.
- [10] S. Jiang, J. Sunarso, W. Zhou, J. Shen, R. Ran, Z. Shao, Cobalt-free  $\text{SrNb}_{0.1}\text{Fe}_{1-x}\text{O}_{3-\delta}$  ( $x = 0.05, 0.1$  and  $0.2$ ) perovskite cathodes for intermediate temperature solid oxide fuel cells, *J. Power Sources* 298 (2015) 209–216.
- [11] D. Ding, X. Li, S.Y. Lai, K. Gerdes, M. Liu, Enhancing SOFC cathode performance by surface modification through infiltration, *Energy Environ. Sci.* 7 (2014) 552.
- [12] F. Dong, M. Ni, M.O. Tade, Z. Shao, Structural and oxygen-transport studies of double perovskites  $\text{PrBa}_{1-x}\text{Co}_2\text{O}_{5+\delta}$  ( $x = 0, 0.05, 0.1$ ) toward their application as superior oxygen reduction electrodes, *J. Mater. Chem. A Mater. Energy Sustain.* 2 (2014) 20520–20529.
- [13] H.U. Anderson, Review of p-type doped perovskite materials for SOFC and other applications, *Solid State Ion.* 52 (1992) 33–41.
- [14] Y. Teraoka, T. Nobunaga, N. Yamazoe, Effect of cation substitution on the oxygen semipermeability of perovskite-type oxides, *Chem. Lett.* (1988) 503–506.
- [15] T. Nagai, W. Ito, T. Sakon, Relationship between cation substitution and stability of perovskite structure in  $\text{SrCoO}_{3-\delta}$ -based mixed conductors, *Solid State Ion.* 177 (2007) 3433–3444.
- [16] Y. Zhu, J. Sunarso, W. Zhou, S. Jiang, Z. Shao, High-performance  $\text{SrNb}_{0.1}\text{Co}_{0.9-x}\text{Fe}_x\text{O}_{3-\delta}$  perovskite cathodes for low-temperature solid oxide fuel cells, *J. Mater. Chem. A Mater. Energy Sustain.* 2 (2014) 15454–15462.
- [17] L. Ge, W. Zhou, R. Ran, S. Liu, Z. Shao, W. Jin, N. Xu, Properties and performance of A-site deficient  $(\text{Ba}_{0.5}\text{Sr}_{0.5})_{1-x}\text{Co}_{0.8}\text{Fe}_{0.2}\text{O}_{3-\delta}$  for oxygen permeating membrane, *J. Memb. Sci.* 306 (2007) 318–328.
- [18] J. Knudsen, P.B. Friehling, N. Bonanos, Effect of A-site stoichiometry on phase stability and electrical conductivity of the perovskite  $\text{La}_{0.59}\text{Fe}_{0.41}\text{O}_{3-\delta}$  and its compatibility with  $(\text{La}_{0.85}\text{Sr}_{0.15})_{0.91}\text{MnO}_{3-\delta}$  and  $\text{Zr}_{0.85}\text{Y}_{0.15}\text{O}_{2.925}$ , *Solid State Ion.* 176 (2005) 1563–1569.
- [19] F.W. Poulsen, Defect chemistry modelling of oxygen-stoichiometry, vacancy concentrations, and conductivity of  $(\text{La}_{1-x}\text{Sr}_x)_y\text{MnO}_{3 \pm \delta}$ , *Solid State Ion.* 129 (2000) 145–162.
- [20] S. Pang, X. Jiang, X. Li, Q. Wang, Z. Su, Q. Zhang, Highly enhanced electrochemical performance of  $\text{PrBa}_{0.92}\text{Co}_2\text{O}_{5+\delta}$  cathode by introducing Ba cationic-deficiency, *Int. J. Hydrogen Energy* 37 (2012) 3998–4001.
- [21] X. Ding, G. Hua, D. Ding, W. Zhu, H. Wang, Enhanced ionic conductivity of apatite-type lanthanum silicate electrolyte for IT-SOFCs through copper doping, *J. Power Sources* 306 (2016) 630–635.
- [22] Y. Zhu, Y. Lin, X. Shen, J. Sunarso, W. Zhou, S. Jiang, D. Su, F. Chen, Z. Shao, Influence of crystal structure on the electrochemical performance of A-site-deficient  $\text{Sr}_{1-x}\text{Nb}_{0.1}\text{Co}_{0.9}\text{O}_{3-\delta}$  perovskite cathodes, *RSC Adv.* 4 (2014) 40865–40872.
- [23] V.V. Kharton, A.V. Kovalevsky, A.P. Viskup, Ceria-based materials for solid oxide fuel cells, *Solid State Ion.* 128 (2000) 117–136.
- [24] H. Zhao, F. Gao, X. Li, C. Zhang, Y. Zhao, Electrical properties of yttrium doped strontium titanate with A-site deficiency as potential anode materials for solid oxide fuel cells, *Solid State Ion.* 180 (2009) 193–197.
- [25] G. Chen, J. Sunarso, Y. Wang, C. Ge, J. Yang, F. Liang, Evaluation of A-site deficient  $\text{Sr}_{1-x}\text{Sc}_x\text{O}_{3-\delta}$  ( $x = 0, 0.02, 0.05$  and  $0.1$ ) perovskite cathodes for intermediate-temperature solid oxide fuel cells, *Ceram. Int.* 42 (2016) 12894–12900.
- [26] S. Pang, X. Jiang, X. Li, Q. Wang, Z. Su, Characterization of Ba-deficient  $\text{PrBa}_{1-x}\text{Co}_2\text{O}_{5+\delta}$  as cathode material for intermediate temperature solid oxide fuel cells, *J. Power Sources* 204 (2012) 53–59.
- [27] D.R.A.G. Pelosato, D. Cordaro, C. Stucchi, Evaluation of Ba deficient  $\text{NdBaCo}_2\text{O}_{5+\delta}$  oxide as cathode material for IT-SOFC, *Electrochim. Acta* 182 (2015) 573–587.
- [28] K. Hansen, K. Hansen, A-site deficient  $(\text{La}_{0.6}\text{Sr}_{0.4})_{1-x}\text{Fe}_{0.8}\text{Co}_{0.2}\text{O}_{3-\delta}$  perovskites as SOFC cathodes, *Solid State Ion.* 178 (2007) 1379–1384.
- [29] T. Chen, S. Pang, X. Shen, X. Jiang, W. Wang, Evaluation of Ba-deficient  $\text{PrBa}_{1-x}\text{Fe}_2\text{O}_{5+\delta}$  oxides as cathode materials for intermediate-temperature solid oxide fuel cells, *RSC Adv.* 6 (2016) 13829–13836.
- [30] L. Ding, L. Wang, D. Ding, S. Zhang, X. Ding, G. Yuan, Promotion on electrochemical performance of a cation deficient  $\text{SrCo}_{0.7}\text{Nb}_{0.1}\text{Fe}_{0.2}\text{O}_{3-\delta}$  perovskite cathode for intermediate-temperature solid oxide fuel cells, *J. Power Sources* 354 (2017) 26–33.
- [31] J.H. Kim, A. Manthiram,  $\text{LnBaCo}_2\text{O}_{5+\delta}$  oxides as cathodes for intermediate-temperature solid oxide fuel cells, *J. Electrochem. Soc.* 155 (2008) B385.
- [32] S.L. Pang, X.N. Jiang, X.N. Li, Q. Wang, Q.Y. Zhang, Structural stability and high-temperature electrical properties of cation-ordered/disordered perovskite  $\text{LaBaCoO}$ , *Mater. Chem. Phys.* 131 (2012) 642–646.
- [33] L. Zhang, G. Yao, Z. Song, B. Niu, W. Long, L. Zhang, Y. Shen, T. He, Effects of Pr-deficiency on thermal expansion and electrochemical properties in  $\text{Pr}_{1-x}\text{BaCo}_2\text{O}_{5+\delta}$  cathodes for IT-SOFCs, *Electrochim. Acta* 212 (2016) 522–534.
- [34] Z. Shao, G. Xiong, J. Tong, H. Dong, W. Yang, Ba effect in doped  $\text{Sr}(\text{Co}_{0.8}\text{Fe}_{0.2})\text{O}_{3-\delta}$  on the phase structure and oxygen permeation properties of the dense ceramic membrane, *Sep. Purif. Technol.* 25 (2001) 419–429.
- [35] J. Mizusaki, M. Yoshihiro, S. Yamauchi, K. Fueki, Nonstoichiometry and defect structure of the perovskite-type oxides  $\text{La}_{1-x}\text{Sr}_x\text{FeO}_{3-\delta}$ , *Solid State Chem* 58 (1985) 257–266.
- [36] H.K. Kammer, A-site deficient  $(\text{Pr}_{0.6}\text{Sr}_{0.4})_{1-x}\text{Fe}_{0.8}\text{Co}_{0.2}\text{O}_{3-\delta}$  perovskites as SOFC cathodes, *J. Electrochem. Soc.* 156 (2009) B1257–B1260.
- [37] J. Zhang, H. Zhao, Y. Li, N. Xu, W. Ding, X. Lu, F. Li, Effects of iron content on the structural evolution, electrical properties and thermochemical stability of  $\text{BaCo}_{0.9}\text{Fe}_x\text{Nb}_{0.1}\text{O}_{3-\delta}$  ceramic membrane, *Int. J. Hydrogen Energy* 35 (2010) 814–820.
- [38] Z. Yang, C. Jin, C. Yang, M. Han, F. Chen,  $\text{Ba}_{0.9}\text{Co}_{0.5}\text{Fe}_{0.4}\text{Nb}_{0.1}\text{O}_{3-\delta}$  as novel oxygen electrode for solid oxide electrolysis cells, *Int. J. Hydrogen Energy* 36 (2011) 11572–11577.
- [39] X. Ding, X. Gao, W. Zhu, J. Wang, J. Jiang, Electrode redox properties of  $\text{Ba}_{1-x}\text{La}_x\text{FeO}_{3-\delta}$  as cobalt free cathode materials for intermediate-temperature SOFCs, *Int. J. Hydrogen Energy* 39 (2014) 12092–12100.
- [40] B. Qian, Y. Chen, M.O. Tade, Z. Shao,  $\text{BaCo}_{0.6}\text{Fe}_{0.3}\text{Nb}_{0.1}\text{O}_{3-\delta}$  perovskite as a new superior oxygen reduction electrode for intermediate-to-low temperature solid oxide fuel cells, *J. Mater. Chem. A Mater. Energy Sustain.* 2 (2014) 15078.
- [41] F. Yang, H. Zhao, J. Yang, M. Fang, Y. Lu, Z. Du, K. Świerczek, K. Zheng, Structure and oxygen permeability of  $\text{BaCo}_{0.7}\text{Fe}_{0.3-x}\text{In}_x\text{O}_{3-\delta}$  ceramic membranes, *J. Memb. Sci.* 492 (2015) 559–567.
- [42] E.D. Wachsman, K.T. Lee, Lowering the temperature of solid oxide fuel cells, *Science* 334 (2011) 935–939.
- [43] Z. Gao, L.V. Moggi, E.C. Miller, J.G. Railsback, S.A. Barnett, A perspective on low-temperature solid oxide fuel cells, *Energy Environ. Sci.* 9 (2016) 1602–1644.
- [44] J.E. ten Elshof, M.H.R. Lankhorst, H.J.M. Bouwmeester, Oxygen exchange and diffusion coefficients of strontium-doped lanthanum ferrites by electrical

- conductivity relaxation, *J. Electrochem. Soc.* 144 (1997) 1060–1067.
- [45] W. He, X. Wu, G. Yang, H. Shi, F. Dong, M. Ni,  $\text{BaCo}_{0.7}\text{Fe}_{0.22}\text{Y}_{0.08}\text{O}_{3-\delta}$  as an active oxygen reduction electrocatalyst for low-temperature solid oxide fuel cells below 600 °C, *ACS Energy Lett.* 2 (2017) 301–305.
- [46] Sherman J. Xu, W.J. Thomson, Oxygen permeation rates through ion-conducting perovskite membranes, *Chem. Eng. Sci.* 54 (1999) 3839–3850.
- [47] B. Wei, Z. Lü, X. Huang, J. Miao, X. Sha, X. Xin, W. Su, Crystal structure, thermal expansion and electrical conductivity of perovskite oxides  $\text{Ba}_x\text{Sr}_{1-x}\text{Co}_{0.8}\text{Fe}_{0.2}\text{O}_{3-\delta}$  ( $0.3 \leq x \leq 0.7$ ), *J. Eur. Ceram. Soc.* 26 (2006) 2827–2832.
- [48] Q. Zhou, T. Wei, Y. Shi, S. Guo, Y. Li, J. Su, H. Ren, Y. Zhu, Evaluation and optimization of  $\text{SrCo}_{0.5}\text{Ta}_{0.1}\text{O}_{3-\delta}$  perovskite as cathode for solid oxide fuel cells, *Curr. Appl. Phys.* 12 (2012) 1092–1095.
- [49] Y. Shen, F. Wang, X. Ma, T. He,  $\text{SrCo}_{1-y}\text{Ti}_y\text{O}_{3-\delta}$  as potential cathode materials for intermediate-temperature solid oxide fuel cells, *J. Power Sources* 196 (2011) 7420–7425.
- [50] B. Qu, W. Long, F. Jin, S. Wang, T. He,  $\text{SrCo}_{0.7}\text{Fe}_{0.2}\text{Ta}_{0.1}\text{O}_{3-\delta}$  perovskite as a cathode material for intermediate-temperature solid oxide fuel cells, *Int. J. Hydrogen Energy* 39 (2014) 12074–12082.
- [51] C. Duan, D. Hook, Y. Chen, J. Tong, R. O'Hayre, Zr and Y co-doped perovskite as a stable, high performance cathode for solid oxide fuel cells operating below 500 °C, *Energy Environ. Sci.* 10 (2017) 176–182.
- [52] L. Ronald, Cook, A.F. Sammells, On the systematic selection of perovskite solid electrolytes for intermediate temperature fuel cells, *Solid State Ion.* 45 (1991) 311–321.
- [53] A.F. Sammells, R.L. Cook, J.H. White, Rational selection of advanced solid electrolytes for intermediate temperature fuel cells, *Solid State Ion.* 52 (1992) 111–123.
- [54] J.A. Kilner, R.J. Brook, A study of oxygen ion conductivity in doped non-stoichiometric oxides, *Solid State Ion.* 6 (1982) 237–252.
- [55] R.J.H. Voorhoeve, J.P. Remeika, L.E. Trimble, Defect chemistry and catalysis in oxidation and reduction over perovskite-type oxides, *Catalytic Chem. Solid-State Inorganics* 272 (1976) 3–21.
- [56] J.R. Wilson, D.T. Schwartz, S.B. Adler, Nonlinear electrochemical impedance spectroscopy for solid oxide fuel cell cathode materials, *Electrochim. Acta* 51 (2006) 1389–1402.
- [57] H. Schichlein, A.C. Müller, M. Voigts, A. Krügel, E. Ivers-Tiffée, Deconvolution of electrochemical impedance spectra for the identification of electrode reaction mechanisms in solid oxide fuel cells, *J. Appl. Electrochem.* 32 (2002) 875–882.
- [58] M.J. Escudero, A. Aguadero, J.A. Alonso, L. Daza, A kinetic study of oxygen reduction reaction on  $\text{La}_2\text{NiO}_4$  cathodes by means of impedance spectroscopy, *J. Electroanal. Chem. Lausanne (Lausanne)* 611 (2007) 107–116.
- [59] Y. Chen, F. Wang, D. Chen, F. Dong, H.J. Park, C. Kwak, Z. Shao, Role of silver current collector on the operational stability of selected cobalt-containing oxide electrodes for oxygen reduction reaction, *J. Power Sources* 210 (2012) 146–153.
- [60] K. Efimov, T. Klande, N. Juditzki, A. Feldhoff, Ca-containing  $\text{CO}_2$ -tolerant perovskite materials for oxygen separation, *J. Memb. Sci.* 389 (2012) 205–215.
- [61] E. Bucher, A. Egger, G.B. Caraman, W. Sitte, Stability of the SOFC cathode material  $(\text{Ba,Sr})(\text{Co,Fe})\text{O}_{3-\delta}$  in  $\text{CO}_2$ -containing atmospheres, *J. Electrochem. Soc.* (2008) 155 B1218.
- [62] W. Chen, C.-s. Chen, L. Winnubst, Ta-doped  $\text{SrCo}_{0.8}\text{Fe}_{0.2}\text{O}_{3-\delta}$  membranes: phase stability and oxygen permeation in  $\text{CO}_2$  atmosphere, *Solid State Ion.* 196 (2011) 30–33.
- [63] M. Li, W. Zhou, Z. Zhu, Highly  $\text{CO}_2$ -tolerant cathode for intermediate-temperature solid oxide fuel cells: samarium-doped ceria-protected  $\text{SrCo}_{0.85}\text{Ta}_{0.15}\text{O}_{3-\delta}$  hybrid, *ACS Appl. Mater. Interfaces* 9 (2017) 2326–2333.
- [64] N.C. Jeong, J.S. Lee, E.L. Tae, Y.J. Lee, K.B. Yoon, Acidity scale for metal oxides and Sanderson's electronegativities of lanthanide elements, *Angew. Chemie* 47 (2008) 10128–10132.
- [65] J. Yi, T.E. Weirich, M. Schroeder,  $\text{CO}_2$  corrosion and recovery of perovskite-type  $\text{BaCo}_{1-x-y}\text{Fe}_x\text{Nb}_y\text{O}_{3-\delta}$  membranes, *J. Memb. Sci.* 437 (2013) 49–56.
- [66] Y. Zhu, Z.G. Chen, W. Zhou, S. Jiang, J. Zou, Z. Shao, An A-site-deficient perovskite offers high activity and stability for low-temperature solid-oxide fuel cells, *ChemSusChem* 6 (2013) 2249–2254.